T.2: Properties of Nanomaterials from First Principles Study

Aparna Chakrabarti (aparna@rrcat.gov.in), Arup Banerjee (banerjee@rrcat.gov.in), C.Kamal(ckamal@rrcat.gov.in), Tapan K. Ghanty (tapang@barc.gov.in)

1 Introduction

There is a recent flurry of activities in understanding the nanostructures - materials with ultra-small dimensions of the order 1 - 100 nm ushering in birth of a new field, now commonly known as *nanoscience*. This field has been attempting to address various important issues ranging from basic science to a variety of technological applications for which the word *nanotechnology* is frequently used. The purpose of *nanoscience* and *nanotechnology* is to comprehend, control, and manipulate objects of a few nanometers in size. Among nano-objects, *nanoclusters* and *nanotubes* occupy a very vital place as they are the basic building blocks of nanodevices. Nanoclusters are complex many-electron systems in between atoms or molecules and the bulk. They are aggregate of atoms or molecules that are too large to be referred to as molecules and too small to be treated like bulk. Being small objects, nanoclusters have very high surface to volume ratio similar to the nanotubes or nanocages of carbon and other materials. It is due to this reason the properties of these nanoclusters are markedly different from those of bulk and also from their constituent atoms. Therefore, they provide an excellent way to study and understand how physical and chemical properties evolve in the transition from an atom to a molecule to a cluster to small particles and finally to a bulk solid. Clusters are different from molecules as they do not have fixed geometry or composition. For example, the water molecule contains one oxygen and two hydrogen atoms, which are placed at a well defined angle to each other. On the other hand, a cluster of alkali metal atom or even water clusters may contain any number of constituent particles. For a given size, clusters typically exhibit a variety of morphologies (Fig. T.2.1).

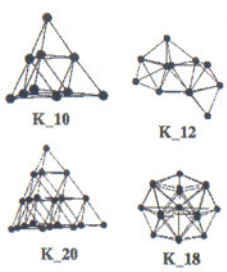

Fig. T.2.1: Some of the configurations with specific symmetries for potassium clusters (K_n : n being 10,12,18 and 20). For example : clusters with atoms 10 and 20 are of T_d symmetry. These structures correspond to optimized geometries.

The properties like geometric structure, binding energy, melting temperature of small clusters containing few hundreds of particles show strong size-dependent behaviour. On the other hand, larger clusters with many thousands of atoms have smoothly varying behaviour, which tends to the bulk limit as size increases. Similarly, the nanotubes and nanocages, mainly due to their large surface to volume ratio, show variety of properties which are very different from their bulk counterpart (Fig. T.2.2).

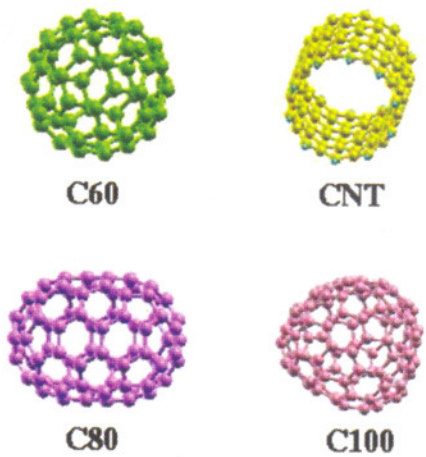

Fig. T.2.2 : Some of the nanotubes and nanocages used in the present work. Carbon nanotubes (CNT) are terminated by hydrogen atoms (blue dots).

The tremendous surge in the reserach work on nanoscience in recent times has been due to the availability of experimental methods for producing nano-objects in a controlled fashion and also characterizing them unambiguously along with the development of sophisticated theoretical tools to handle such finite fermion systems at *abinitio* level. We note here that nanoscience is a field which requires a synergy between the experiments and theoretical methods for both characterizing and understanding the properties of nano-objects. Our research work in the area of nanoscience is primarily aimed at theoretical understanding of various ground-state electronic and optical response properties of variety of nano-objects. In this connection we emphasize here that nano-objects, even a cluster of few atoms is a complex many-electron system especially from theoretical point of view. For correct description of many-electron systems, it is necessary to adopt methodologies which take into account electron-electron correlation in an efficient way and this is also essential for correct determination of optical response properties. Density functional theory (DFT) and its time dependent counterpart time-dependent DFT (TDDFT) provide efficient ways to perform both model-based and *ab initio* calculations taking into account electron-electron interaction and that is why

these two methods have found wide applications in determining electronic structures and response properties of atoms, molecules, clusters and solids. We wish to mention here that there also exist a number of wave-function-based qunatum chemical methods for calculating electronic structure and optical response properties at varying levels of sophistication taking electron correlation into account. However, these methods turn out to be computationally very expensive for systems containing more than few atoms. On the other hand, DFT/TDDFT when adequatly tested, can be of very high accuracy and significantly less cumbersome, from the computational point of view, making it possible to handle much larger clusters. For example, calculations on metal clusters including transition metals and noble metals with more than hundred atoms have been reported in the literature. Although DFT/TDDFT methods are exact in principle but calculations by these methods are performed with approximate forms for the exchange-correlation (XC) term. The choice of exchange-correlation has to be tested for each system. In next section we discuss the effect of different exchange-correlation functionals in determining some of the properties.

We carry out theoretical calculations of various properties of metal (Na_n, K_n, and $Au_{19}X$, X = Li, Na, K, Rb, Cs, Cu, Ag), semiconductor (Ga_nP_n), carbon (C_{20}, C_{60}, C_{80} and C_{100}) clusters and carbon nanotubes (CNT). For each system we first carry out DFT-based geometry optimization calculation to obtain energetically stable structures. Using these optimized structures we first calculate ground-state properties like binding energy (BE), HOMO-LUMO gap, ionization potential (IP), and electron affinity (EA) to characterize their stability. Experimentally optical response properties like dipole polarizability and VIS-UV optical absorption spectrum are routinely measured for characterization of nanosystems. Keeping this in mind we devote our significant research endeavour on calculating these response properties by employing TDDFT. The van der Waals interaction coefficient (C_6) is associated with the interaction potential which decays as R^{-6}(where R is the intermolecular distance) and it describes the dipole-dipole interaction between the two polarizable systems. We note here that in principle, ground state DFT should yield the exact ground-state properties including the long range van der Waals energies. However, the widely used local density approximation (LDA) and generalized gradient approximation (GGA) XC functionals as well as popular hybrid functionals fail to reproduce the van der Waals energies. This is due to the fact that the LDA and GGA functionals cannot describe the correlated motion of electrons arising from Coulomb interaction between distant non overlapping electronic systems. It is only recently that attempts have been made to obtain van der Waals energies directly from the ground-state energy functional through systematic improvements of the effective Kohn-Sham potential. On the other hand, it is possible to make reliable estimates of the van der Waals coefficient C_6 directly by using expressions which relate this coefficient to the frequency dependent dipole polarizabilities at imaginary frequencies which can be computed from TDDFT using common functionals. We follow the latter route for the calculation of this coefficient. We employ TDDFT to calculate the frequency dependent dipole polarizability for a range of frequencies and then use Casimir-Polder expression to calculate C_6 for interaction between various pairs of nano-objects of different sizes and chemical compositions.

All the calculations of various ground-state and response properties of the above-mentioned systems have been performed by employing Amsterdam Density Functional (ADF) program package for DFT/TDDFT based computations, and GAMESS electronic structure code for carrying out post-Hartree-Fock Moeller-Plesset (MP2) and coupled cluster (CCSD(T)) calculations. For each type of nano-objects, we optimize geometries of several possible isomers (wherever applicable) of the clusters. The geometry optimizations of all the systems have been performed through DFT based calculations by employing appropriate basis set. For most of the systems, we use triple ς Slater-type orbital (STO) basis set with two added polarization functions (TZ2P basis set of ADF basis set library).

2 Results and Discussion

2.1 Effect of exchange-correlation potentials

The exchange-correlation (XC) functional which are used in DFT/TDDFT calculations are extremely important. These potentials can affect different properties, and a wrong choice of an XC potential can lead to inaccurate prediction of properties. Below we discuss our results for some cases. We have calculated the static dipole polarizability ($\alpha(0)$) of various clusters made of Gallium Phosphide (Ga_nP_n) as well as alkali metals sodium (Na_n) and potassium (K_n) atoms, by employing various *ab initio* wave function based methods and DFT/TDDFT method[1,2,3]. A systematic investigation is carried out to analyse the performance of different XC functionals used in DFT/TDDFT method in determining static dipole polarizability of these clusters. The results for most stable isomers of Ga_nP_n show that, the DFT/TDDFT method with different XC functionals underestimate the values of polarizability in comparison to the results of MP2 method, which is a wave function based method and is known to yield accurate results[1]. Among the several XC functionals, the performance of GGA XC has been the best when compared to the results from MP2 method. In comparison to the results produced by the MP2 method, the values of polarizability obtained by the DFT/TDDFT calculation with a model potential - SAOP - possessing

correct behaviors both in the asymptotic and inner regions of the molecule, are found to be worse than those obtained with the LDA and GGA XC functionals.

In this connection we mention that the correct asymptotic behavior of SAOP is capable of yielding quite accurate results for the low lying excited states. However, for high lying excited states it is not quite that accurate. This may be one reason for the discrepancy between the results for polarizability obtained via TDDFT (XC SAOP) and MP2 methods. On the other hand, the closeness of LDA and GGA results to MP2 data may be attributed to the following. The LDA and GGA XC potentials underestimate the contributions to the polarizability arising from transition to bound Rydberg type states and overestimate those from continuum. The cancellation of errors in these two contributions to the polarizability sometimes yields good results for it accidentally[1]. Therefore, the closeness of LDA and GGA results with MP2 values in some systems, as for example here, may be fortuitous. However, no such cancellations of errors occur when excited states are obtained with SAOP XC potential. Hence it may be due to this lack of cancellation together with inaccuracy in predicting high lying excited states by SAOP that leads to results for the polarizability which deviate more from MP2 data than the corresponding LDA and GGA values in case of Ga_nP_n clusters[1].

Now it is important to note here that unlike III-V semiconductor clusters, for alkali metal clusters consisting of Na and K atoms, the values of polarizability obtained by employing SAOP [2,3] are very close to data from accurate wave function based methods (MP2 and CCSD(T)) as well as experimental data available in the literature. Moreover, for these systems the SAOP results are also significantly higher than both LDA and GGA values. For these systems, only few low lying excited states contribute to the polarizability as these few states are sufficient to saturate the oscillator strength of excitations. It is exactly these low lying states which are well reproduced by SAOP, thus giving very accurate values of polarizability of alkali metal clusters. *Summary : Hence, our present study on clusters made of different classes of materials signifies the importance of understanding the underlying aspects of each XC potential used in any first principles calculations to obtain various ground state or response properties.*

2.2 Interesting size-to-property relationship

2.2.1 $\bar{\alpha}$ and C_6 of alkali metal clusters

We calculate the $\bar{\alpha}(0)$ of different atomic and molecular clusters using DFT/TDDFT. In this subsection, we present the data for the alkali metal atom clusters, consisting of Na and K atoms[2,3].

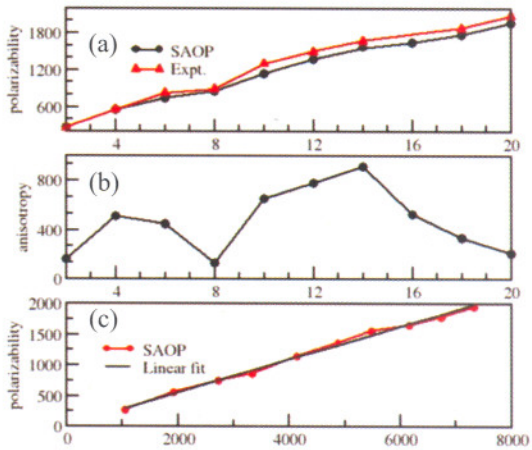

Fig. T.2.3: Results of static polarizability and anisotropy in polarizability for Na atom clusters. Upper panel shows comparison of our theoretical and experimental data from literature for clusters with upto 20 atoms. Middle panel shows the anisotropy. The x-axis for upper and middle panels is the number of atoms in the cluster. Bottom panel shows polarizability as a function of volume in au^3. Lines are guides to the eyes. Linear fit to volume is represented by black line.

Fig.T.2.3 (upper panel) shows the plot of $\bar{\alpha}(0)$ of Na atom clusters, Na_n, n being an even number and varying from 2 to 20. Along with the calculated results we also plot the corresponding experimental results obtained from the literature. The data in Fig. T.2.3 (upper panel) clearly shows that, though the results obtained by *abinitio* method are slightly lower than the corresponding experimental data, the two data, specifically the increasing trend of the $\bar{\alpha}(0)$ with the number match very well with each other. The clusters under present study are essentially non-spherical in nature, consequently the polarizability tensors are anisotropic. It is then natural to investigate how the anisotropy in polarizablity evolves with the size of the cluster. For this purpose, we carry out calculations of anisotropy in polarizabilty given by

$$|\Delta\alpha| = \left[\frac{3\tau ra^2 - (\tau ra)^2}{2} \right]^{1/2}$$

where α is the second-rank polarizability tensor. The middle panel of Fig.T.2.3 shows the plot of anisotropy $\Delta\alpha$ of Na atom clusters as a function of n. It is interesting to see that there is a clear size (or number)-to-property relationship. The clusters with magic number of atoms (n= 2, 8, 20) show a very small anisotropy in α, which corroborates with the fact that the clusters with magic number of atoms are more symmetric in structure, naturally leading to a smaller value of anisotropy compared to the other clusters with non-magic number of atoms. The bottom panel of Fig.T.2.3 shows the plot of $\bar{\alpha}(0)$ as function of total cluster volume. It is interesting to see that a good linear fitting with the volume exists with a correlation coefficient close to one. This indicates that the $\bar{\alpha}(0)$ value

exhibits a linear dependence on the volume of the cluster as has been observed recently in the literature for clusters of smaller number of atoms (n less than 10). In Fig.T.2.4, we show the same properties for K_n, n being from 2 to 20. Top, middle and bottom panels show $\bar{\alpha}(0)$, $\Delta\alpha$ and the volume dependence of $\bar{\alpha}(0)$, respectively. It is observed that the results are very similar and the trends are same in the clusters both made of alkali metal atoms.

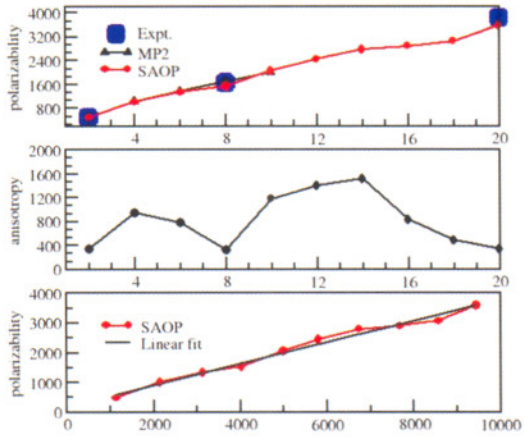

Fig. T.2.4: Results of static polarizability and anisotropy of polarizability for K atom clusters. Upper panel shows comparison of our theory and available experimental data (for n=2, 8 and 20) from literature for clusters with upto 20 atoms. Middle panel shows the anisotropy. The X-axis for upper and middle panels is the number of atoms in the cluster. Bottom panel shows polarizability as a function of volume in au^3. Lines are guides to the eyes. Linear fit to volume is represented by black line.

Furthermore, we discuss now another interesting size-to-property relationship. In the literature, there are contradictory findings regarding the evolution of the polarizability with the size of the cluster with respect to the polarizability of the bulk. Our calculations of static dipole polarizability per atom for gallium phosphide clusters (Ga_nP_n) show that the polarizability value reaches the bulk limit from above as the size of the clusters increases [1].

After finding the correct trend in the $\bar{\alpha}(0)$ and $\Delta\alpha$ values as well as establishing the goodness of the approach of calculating these properties, we now move on to discuss about the van der Waals (vdW) interaction between these clusters. Now we focus our attention on the scaling behaviour of the van der Waals coefficient with the voume of the clusters (to establish any size-to-property relationship). We calculate the same for Na clusters (Na_n)[2]. We demonstrate that C_6 vary quadratically with the volume of the clusters. The same has been observed for K_n clusters as well[4]. It is important to note that this scaling behavior is applicable for both spherical as well as non-spherical geometries. The scaling behavior of C_6 can be understood by considering the expression for it within London approximation. Within this approximation the dispersion coefficient C_6 between two molecules is represented in terms of an effective or a characteristic frequency ω and the static polarizability as $C_6 = \frac{3}{4}\hbar\omega_1 \bar{\alpha}(0)^2$

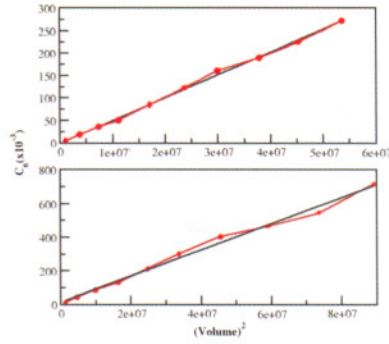

Fig. T.2.5 : van der Waals coefficients as a function of square of volume in atomic units. Upper and bottom panels show the same for Na and K atom clusters, respectively. The data are plotted with red dots (joined with lines for guide to the eye), linear fit to square of the volume is represented by black lines.

Since static polarizability is known to vary linearly with volume[2,3], then under the assumption that the characteristic frequencies do not vary much with the size of the clusters, it is expected that C_6 scales quadratically with the volume. To check the validity of this assumption, we present here the characteristic frequencies ω of potassium clusters by employing above equation using the values of C_6 and $\alpha(0)$ obtained with the asymptotically correct XC potential - the statistical average of orbital potential (SAOP)[4]. We find that these frequencies lie within a range from 0.061 to 0.078 a.u. around the mean of 0.070 a.u.. This narrow distribution of ω values around its mean value warrants the above mentioned assumption and consequently a very good linear fit between C_6 and square of the volume of the cluster has been obtained. This is elucidated in Fig.T.2.5 where we plot C_6 for both Na_n (upper panel) and K_n (lower panel) clusters obtained as a function of *(volume)*^{2} along with the least square fitted line. It can be clearly seen from Fig. T.2.5, that a linear relation exists and a good fitting is obtained with the correlation coefficient value close to one (above 0.99). This suggests that both for Na [2] and potassium clusters[4], a good linear correlation exists between the C_6 and the square of the cluster volume. *Summary : Hence, our results on $\bar{\alpha}(0)$ and C_6 for different clusters establish important examples of the interesting size-to-property relationship in case of nanoclusters, as elucidated above.*

2.2.2 $\bar{\alpha}(0)$ and C_6 of carbon nanostructures

We calculate the long range dipole-dipole dispersion coefficient, the van der Waals coefficient, C_6, between different finite carbon cages and finite-length single-walled H-terminated carbon nanotubes (CNT) with different size and chirality, containing maximum about 100 atoms[5]. Our aim is to accurately estimate the comparative strength of the long-range van der Waals interaction between these carbon nanosystems (CNS). It is established that correct behavior of the exchange-correlation potential, specifically in the asymptotic regime, plays a crucial role in the accurate determination of the response properties. Hence we employ in our calculations the asymptotically correct exchange-correlation potential SAOP. First we report the average static polarizabilities of the CNTs. From our calculations, we find that for the CNTs studied in this work, the average static polarizability increases with the length of the tube in a non-linear fashion.

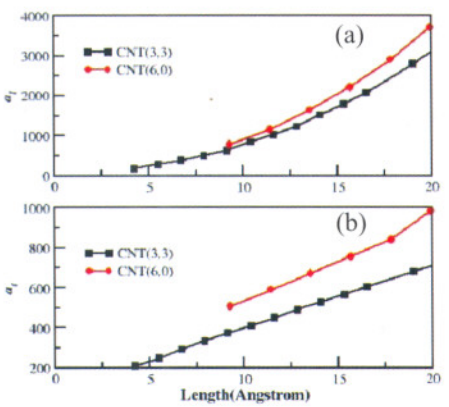

Fig. T.2.6: Plot of (a) longitudinal and (b) transverse components of static polarizability as a function of length of the tube for two typical nanotubes, chirality index for the zig-zag tube is (6,0) and the arm-chair tube is (3,3). Symbols correspond to the data and lines are guide to the eyes.

Fig. T.2.6 shows the parallel or longitudinal and the perpendicular or transverse components of the polarizability for two prototype tubes, one an arm-chair tube (CNT(3,3)) and another a zig-zag tube (CNT(6,0)), as a function of length of the tubes. All the tubes studied show the same trend. The upper panel of Fig.T.2.6, which gives the parallel component of polarizability for the two prototype tubes shows that it varies non-linearly with the length which is similar to the length-dependence of the total polarizability. On the other hand, in the lower panel of Fg.T.2.6, the perpendicular component is seen to have a linear dependence with length of the tube. We find that these quasi one-dimensional structures also show large anisotropy in polarizabilty. In calculating C_6, we need to calculate and use the frequency dependent polarizabilities. The C_6 values increase linearly with the diameter of the CNTs, while these values show a quadratic dependence on the length of the tubes, as is shown in Fig.T.2.7. It has also been observed that there is a quadratic dependence of the C_6 with the polarizability values for both the cages and the tubes. It is observed that the zigzag tubes have larger polarizability and C_6 compared to the armchair tubes[5]. This is due to the fact that zigzag tubes have more number of bonds along the tube axis, making them more polarizable which in turn leads to stronger dispersion interaction between the zigzag tubes as is observed from our calculations. The loosely bound π-electrons play a major role in the polarizability of carbon nanostructures. The bigger the system in size the larger is the number of the π-electrons and the volume over which these electrons are spread. Hence, the long-range interaction in these highly polarizable systems with a large number of carbon atoms is expected to be strong. The carbon cages are less polarizable than the CNTs due to the compact shape of the former, hence we observe that the cages with similar number of atoms are having polarizability and C_6 (Fig. T.2.7) values which are much lower as compared to the corresponding mean values for CNTs. For nanostructures with 60 and 80 atoms, it is found that the C_6 and polarizability are about 40 - 50 % lower in the cages compared to the tubes[5]. *Summary : Our observation of nonlinear increase of the C_6 values of the carbon nanostructures with length implies a much stronger vdW interaction between the longer carbon nanostructures compared to the shorter ones. The present result can be useful in studies of cluster-cluster and cluster-surface interactions in carbon-based systems at the nanometer level as well as in understanding the formation of superstructures of these. We also note that the existence of large anisotropy in polarizability in carbon nanotubes can play an important role in electric field aligned growth of these systems.*

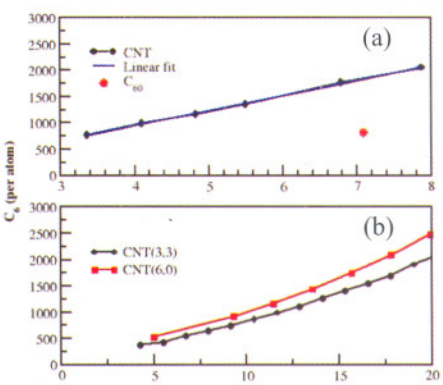

Fig. T.2.7: Plot of van der Waals coefficients : (a) as a function of the diameter (in Angstorm) of diffrent CNTs with 60 carbon atoms, as well as (b) number of atoms for two typical nanotubes, CNT(6,0) and CNT(3,3). In upper panel data are shown by symbols (lines as guide to the eyes) and linear fit to the data is shown by a line. The C_6 for C_{60} is given by red star.

2.3 van der Waals coefficients between CNS and alkali atom clusters as well as small molecules

In this section, we first report the van der Waals interaction, in terms of the C_6 coefficients, between the carbon cage C_{60} and alkali metal atom clusters, namely, Na_n as this force plays an important role in describing many physical and chemical phemomena. Table 1 gives our present results as well as other theoretical results along with the experimental data fitted with London's formula which are available in the literature [6]. Model XC potential SAOP has been used for these calculations due to the reasons discussed above. The values of C_6 between the C_{60} and Na_n are seen to agree well with the earlier theoretical as well as the experimental results; these data are seen to lie well within the experimental error bars when compared to the experimental results available in the literature [6].

Table T.2.1: Results for $C_6 \times 10^3$ between sodium clusters and C_{60} molecule in atomic units. The theoretical results obtained via B3PW91 XC potential and the experimental results are taken from literature.

Nan	SAOP	B3PW91	EXPERIMENTAL
2	15.27	15.36	17.62±5.11
4	30.55	29.94	25.05± 7.44
6	43.42	43.33	38.91± 12.06
8	53.36	54.33	55.01±15.95
10	68.39	65.67	63.71±19.75
12	82.00	81.81	92.52±28.68
14	94.38	98.25	108.3± 33.56
16	103.7	-	117.8±37.72
18	113.7	111.7	139.0±43.10
20	134.7	124.0	169.2±52.45

All the results indicate an increase in C_6 value as the size of the cluster increases. Furthermore, the knowledge and accurate estimate of the vdW interaction between the carbon-based nanomaterials with large surface-to-volume ratio and different molecules of environmentally important gases can be highly important for possible practical applications of the carbon nanostructures as absorbers of these molecular gases. Therefore, we obtain an accurate estimate of the vdW coefficients between different gas molecules and carbon cages as well as finite-length carbon nanotubes using the state-of-the-art TDDFT method and SAOP XC potential [5,7]. It is found that the rare gas atoms have low vdW coefficient while the greenhouse gases - carbon dioxide, methane and nitrous oxide, show quite high C_6 values, when compared to rare gases or most of the other molecules[5,7].

Summary :Our accurate ab initio estimate of the van der Waals interaction in terms of the C_6 coefficients can help in microscopic understanding of the interaction and consequently some physical, chemical or biological processes involving these molecular or cluster systems with the carbon nanostructures. However, we note that, there are two competing forces those come into play if a molecule interacts with a carbon nanostructure - first is the long-range interaction that is characterized by the C_6 coefficient, second is the repulsive interaction arising due to the overlapping charge distributions of the two systems. Hence it is not possible to infer from the results of polarizability and C_6 alone as to whether the molecules will adhere to the carbon nanostructures exohedrally or not. Furthermore, the kinetic aspects which are also closely involved in a physisorption process cannot be addressed and accounted for from the present study[5,7].

2.4 Effect of alkali metal atom doping in Au_{20}

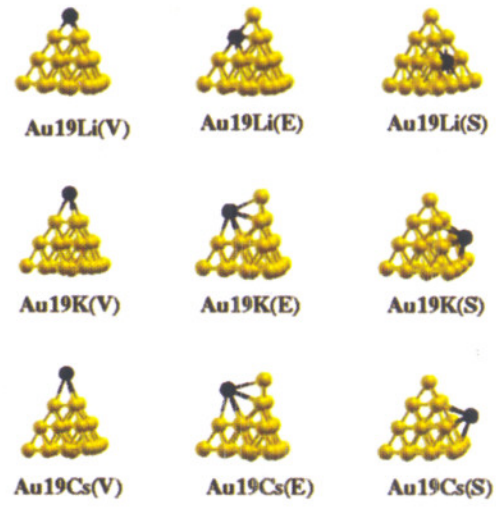

Fig. T.2.8 : Some of the gold clusters, with a replacement doping of one alkali metal atom. V, E and S represents vertex, edge and surface sites of the gold cluster. Li=Lithium, K=Potassium, Cs=Cesium.

Due to the relatively free-electron nature of the alkali metal atoms the doping of nanoclusters with them and the changes in the properties thus can be of interest for various applications. In this section we will report the results of a study on alkali-metal atom doped nanoclusters of gold atoms. In our study on doped gold cluster we mainly investigated how the stability and chemical inertness of highly stable Au_{20} cluster are affected when a gold atom in it is replaced by an alkali atom. To this end we carry out a systematic study of electronic properties of doped neutral gold clusters $Au_{19}X$ (X

= Li, Na, K, Rb, and Cs). In the tetrahedral structure of the Au_{20} cluster, the sites can be grouped into three categories : four equivalent vertex sites, four equivalent face-centered or surface sites, and twelve equivalent sites located on the edges. To study the doped clusters we replace a single gold atom from one of these three unique sites by an alkali atom (Li, Na, K, Rb, Cs), we also study coinage metal atoms (Ag, Cu). But here we report only the case of alkali metal atoms. The ground state structures and the electronic properties of doped and undoped gold cluster with 20 atoms (Fig. T.2. 8), have been calculated by employing *abinitio* method within the realm of scalar relativistic DFT. The relativistic effects are taken into account. The starting geometries of $Au_{19}X$ for structure optimization are generated from tetrahedral geometry of Au_{20} cluster by replacing the gold atom from one of the three distinct groups mentioned above by an alkali atom. These structures are then optimized by employing DFT based geometry optimization scheme with PW91 XC potential within GGA and TZ2P basis set. The optimized structures of $Au_{19}X$ clusters based on tetrahedral geometry as obtained from our calculations are displayed in Fig. T.2.8. The optimized stucures of clusters with dopant atoms located at surface and the vertex locations possess C_{3v} symmetry whereas for dopant atoms located at edges have C_s symmetry. In order to check the stability of these geometries we carry out vibrational analysis. None of the clusters considered in this work possesses any imaginary harmonic vibrational frequencies, indicating stable structures for all. We observe that the Cs atom substituted clusters show maximum deviation from the tetrahedral structure, hence these are expected to be least stable structures; Li atom substituted clusters are among the least distorted ones compared to the pure Au_{20} structure (Fig. T.2. 8) and hence are more stable [8]. In order to make our search for the stable isomers of doped $Au_{19}X$ clusters more exhaustive, we also consider cage-like structures in which dopant atom X is located at an endohedral position. To analyze and compare the stability and the chemical inertness of the doped clusters with the pure Au_{20} cluster, we calculate the charge population, BE energy per atom, the interaction energy (IE) of the substituted atom with the Au_{19} cluster, vertical IP (VIP) and EA (VEA), and the HOMO-LUMO gaps of the doped clusters. It is observed that the dopant atoms change the atomic charge of a particular site considerably. For the surface doping, the vertex atoms undergo the maximum change in the charge distribution. A substitution at the vertex site causes the maximum change in the charge for the adjacent edge atoms. Doping at any edge site leads to the maximum changes in the overall charge distribution, affecting all the atoms. We observe that for gold clusters doped with Li (located at the edge and surface positions), the BE per atom is higher than the corresponding value for Au_{20}. For all other alkali atoms the BE is lower than that for the Au_{20} cluster. On the basis of the BE and geometrical analysis, it is established that the clusters with dopant atom located at the surface are the most stable structures as compared to the edge and vertex sites. We note that for a particular dopant atom X, VIP follows the trend VIP(V) < VIP(E) < VIP(S). For alkali metal atom doping we find that, both VIP and HOMO-LUMO gap decrease as we move down the group from Li atom to Cs atom. Like VIP, VEA also follows a similar trend. The BE analysis shows that for small dopant atoms like Li, Na, few cage-like endohedral structures of $Au_{19}X$ clusters have stability comparable to the corresponding exohedrally doped clusters. However, among all the structures considered in this work exohedrally doped $Au_{19}X$ clusters with dopant atom (X = Li, Na) sitting at one of the surfaces of tetrahedral (Au_{20}) structure correspond to the most stable isomers of $Au_{19}X$. For Li, an equally stable (BE same as that of corresponding exohedral stucture) cage-like isomer with C_{3V} symmetry and endohedral doping is also found. For larger alkali atoms (K, Rb, and Cs) all the cage-like structures with endohedral doping are found to be significantly less stable than the corresponding exohedral structures. *Summary : We conclude that the replacement of an Au atom at the surface site of the tetrahedral structure of the pure Au_{20} cluster by a Li atom among other alkali metal atoms results in a highly stable cluster. Therefore it is expected that an anion of this cluster ($Au_{19}Li^-$) might be highly reactive and a potential candidate for catalysis.*

Acknowledgements

The authors thank Dr. P. D. Gupta, Dr. S. M. Oak, Dr. S. C. Mehendale, Dr. T. Mukherjee and Dr. S. K. Ghosh for their encouragement and support. The help and support of scientific computing groups and computer centres of RRCAT and BARC are acknowledged with thanks.

References

1. C. Kamal, T. K. Ghanty, A. Banerjee, A. Chakrabarti, J. Chem. Phys. 130, 024308, 2009.
2. A. Banerjee, A. Chakrabarti, T. K. Ghanty, J. Chem. Phys. 127, 134103, 2007.
3. A. Banerjee, T. K. Ghanty, A. Chakrabarti, J. Phys. Chem. (A) 112, 12303, 2008.
4. A. Banerjee, A. Chakrabarti, T. K. Ghanty, Int. J. of Quant. Chem. 109, 1376, 2009.
5. C. Kamal, T. K. Ghanty, A. Banerjee, A. Chakrabarti, J. Chem. Phys. 131, 164708, 2009.
6. A. Banerjee, J. Autschbach, A. Chakrabarti, Phys. Rev. A 78, 032704, 2008.
7. C. Kamal, T. K. Ghanty, A. Banerjee, A. Chakrabarti, RRCAT Newsletter, 23, 18, 2010.
8. T. K. Ghanty, A. Banerjee, A. Chakrabarti, J. Phys. Chem. (C) 114, 20, 2010.